Stem Cell Reports
Article

ISSCR

OPEN ACCESS

iPSC-Derived Retina Transplants Improve Vision in *rd1* End-Stage Retinal-Degeneration Mice

Michiko Mandai,[1,*] Momo Fujii,[1] Tomoyo Hashiguchi,[1] Genshiro A. Sunagawa,[1] Shinichiro Ito,[1] Jianan Sun,[1] Jun Kaneko,[1] Junki Sho,[1] Chikako Yamada,[1] and Masayo Takahashi[1]

[1]Laboratory for Retinal Regeneration, RIKEN Center for Developmental Biology, 2-2-3, Minatojima-minamimachi, Chuo-ku, Kobe, Hyogo 650-0047, Japan

*Correspondence: mmandai@cdb.riken.jp

http://dx.doi.org/10.1016/j.stemcr.2016.12.008

SUMMARY

Recent success in functional recovery by photoreceptor precursor transplantation in dysfunctional retina has led to an increased interest in using embryonic stem cell (ESC) or induced pluripotent stem cell (iPSC)-derived retinal progenitors to treat retinal degeneration. However, cell-based therapies for end-stage degenerative retinas that have lost the outer nuclear layer (ONL) are still a big challenge. In the present study, by transplanting mouse iPSC-derived retinal tissue (miPSC retina) in the end-stage retinal-degeneration model (*rd1*), we visualized the direct contact between host bipolar cell terminals and the presynaptic terminal of graft photoreceptors by gene labeling, showed light-responsive behaviors in transplanted *rd1* mice, and recorded responses from the host retina with transplants by ex vivo micro-electroretinography and ganglion cell recordings using a multiple-electrode array system. Our data provides a proof of concept for transplanting ESC/iPSC retinas to restore vision in end-stage retinal degeneration.

INTRODUCTION

Although fetal retinas have been transplanted into patients with retinal degeneration, there is no conclusive evidence that these transplants can restore visual function (Radtke et al., 2008). Recently, Pearson et al. (2012) demonstrated that postnatal photoreceptor precursor cells can functionally integrate into the outer nuclear layer (ONL) of *Gnat*$^{-/-}$ mice and restore visual function; in these mice, rod photoreceptors are not functional but transplanted rod cells can restore scotopic visual function in a dose-dependent manner. Gonzalez-Cordero et al. (2013) then reported that mouse embryonic stem cell (mESC)-derived photoreceptor precursors can integrate into the ONL of mice retina. These reports, together with a number of reports describing protocols to differentiate retinal tissue from human ESCs or induced pluripotent stem cells (iPSCs) (Kuwahara et al., 2015; Nakano et al., 2012), provided a basis for developing cell-based therapies for retinal degenerative diseases. More recently, however, Pearson's and another group have reinterpreted their work, as new evidence has emerged that the functional restoration after photoreceptor transplantation had been more likely the result of biomaterial transfer from the transplanted cells to the local photoreceptor cells in the host ONL, rather than direct integration of the graft cells (Pearson et al., 2016; Santos-Ferreira et al., 2016). These reports brought us back to the initial question of whether the transplanted photoreceptors could make synapses with adult host retinal cells.

In clinical practice, cell-based therapies would primarily target end-stage retinas that have lost the ONL, leaving the secondary retinal neurons missing their partners for signal input. Therefore, the end-stage retinas can be considered to be in a different environment for graft cells from those of disease models retaining ONL that were used in the previous studies. Recent studies using photoreceptor cell suspension in end-stage retinas, which have lost the ONL, indicated possible light response by pupillary reflex and behavior tests, although direct evidence of light response from the graft cells or synaptic function is still lacking. These graft photoreceptors did not develop mature morphology with outer segments or organized ONL structure that is important for photoreceptors to efficiently respond to light (Barnea-Cramer et al., 2016; Singh et al., 2013). In addition, retinal grafts in the form of cell suspension or microaggregates did not generally survive for long, whereas a retinal graft sheet in a clinical trial was observed to survive 3 years after the transplantation (del Cerro et al., 2000; Mandai et al., 2012; West et al., 2010). Reconstruction of a structured ONL would definitely be ideal in these cases, but it has not been clearly demonstrated that a structured, retina-like sheet can restore visual function. The difficulty of proving that visual function is present in mice and rats adds to the challenge of developing effective therapies for retinal degeneration.

We previously reported that 3D retinal tissue differentiated from mESC or mouse iPSC (miPSC) retina can develop a structured ONL of fully mature photoreceptors with outer-segment structures when transplanted into *rd1* end-stage retinal-degeneration model mice, possibly by forming synapses with host bipolar cells (Assawachananont et al., 2014). These grafts can integrate with or without the presence of graft inner cells between the host inner nuclear layer (INL) and the graft ONL; the latter most closely resembles the natural retina and appears most promising for restoring visual function, although this has not been

demonstrated. More recently, we also showed that hESC retina can similarly develop and mature after transplantation in the ONL-lost retinal-degeneration models of rats and monkeys in a similar manner (Shirai et al., 2015). Thus, the current question is whether the integrated ONL responds to light and transmits signals to host upper neurons in the end-stage host retina, especially to the retinal ganglion cells (RGCs) that subsequently transmit the neural signals to the brain.

In the present study, we assessed the visual function in *rd1* mice with miPSC-retina transplants using a refined protocol on shuttle-avoidance tests, analyzed the light-responsive function in retinal transplants using ex vivo micro-electroretinogram (mERG) and RGC recordings, and examined the host-graft contact directly by genetically labeling the graft photoreceptor terminals. Our data provide a proof of concept for transplanting ESC/iPSC retinas to treat end-stage retinal degeneration. Here we also demonstrate practical, reliable methods for qualitatively and quantitatively assessing visual function in regenerative studies in mice.

RESULTS

Visualization of Direct Contact between Host Bipolar Cells and Synaptic Terminals of Graft Rod Photoreceptors

To clearly identify direct host-graft integration, we generated iPSC lines that express CtBP2-tdTomato at photoreceptor synaptic terminals after differentiation (Nrl-GFP/ROSA::Nrl-CtBP2-tdTomato) (Figures S1A–S1C). We also prepared an end-stage retinal-degeneration model mouse that expresses GFP in rod bipolar cells (L7-GFP/*rd1*) by crossing *rd1-2J* and L7-GFP mice. We found that three of the Nrl-GFP/ROSA::Nrl-CtBP2-tdTomato lines differentiated to form optic vesicles similar to those we described previously (Figure S1D). A retinal sheet cut out from an optic vesicle on differentiation day 13 (DD13) was transplanted into each L7-GFP/*rd1* mouse; after transplantation, the grafts developed an Nrl-GFP-positive, rhodopsin-positive ONL with outer-segment-like structures on DD35, as we showed previously, although GFP positivity was weaker compared with later DDs (Figures 1A and 1A′) (Assawachananont et al., 2014), and L7-GFP-positive host bipolar terminals contacted CtBP2-tdTomato-positive graft regions. CtBP2-tdTomato, which was present along the margins of the Nrl-GFP-positive graft ONL, colocalized with anti-CtBP2 immunostaining (Figures 1B–1B‴). CtBP2-tdTomato also clustered at the tips of graft bipolar dendrites where they formed intra-graft synapses with Nrl-GFP-positive photoreceptors (Figure S2A). These findings indicate that tdTomato represents the CtBP2 expression at graft photoreceptor terminals. Some terminals in the host retina were negative for tdTomato (Figure 1C, arrows), suggesting that they were the remnants of host photoreceptors. We also found the outgrowth of tdTomato-positive graft CtBP2 into the host synaptic layer (Figures 1D–1D‴, arrows). We then more closely studied the contact between L7-GFP-positive host bipolar cells and CtBP2-tdTomato on graft photoreceptors. In the L7-GFP retina, GFP-positive bipolar cells mostly overlapped with protein kinase Cα (PKCα)-positive bipolar cells, but in L7-GFP/*rd*, GFP expression was reduced in variable degree in PKCα-positive cells in some parts of the retina (Figures S2B and S2C). GFP-positive host bipolar cells sometimes extend their dendrites even through the remaining graft INL to reach tdTomato-positive graft CtBP2 (Figure 2A). Although it was sometimes difficult to distinguish graft and host terminals of either bipolar cells or photoreceptors, our labeling approach offers evidence of direct contact between the host L7-GFP-positive bipolar cell dendrites and tdTomato-positive graft photoreceptor synaptic terminals, such as seen between bipolar dendrites and CtBP2 in L7-GFP wild-type retina (Figures 2B and 2C–2C‴). We also stained one of the postsynaptic markers, CACNA1s, that was reported to localize at postsynaptic ribbon synapses and recently identified to cross-react with GRP179 (Hasan et al., 2016; Specht et al., 2009; Tummala et al., 2014). The presence of CACNA1s was observed at the tips of bipolar cells in a wild-type retina (Figure 2D), and CACNA1s immunoreactivities were also present coupled with graft presynaptic terminal, CtBP2-tdTomato, at the tips of L7-GFP-positive bipolar cells, indicating the presence of host-graft synaptic formation (Figures 2E and 2E′). We also observed dendrite tips of PKCα-positive/GFP-negative bipolar cells in the host retina that were in contact with graft regions labeled by CtBP2-tdTomato (Figure S2D), implying that host-graft contact occurred more frequently than was reported by our labels.

Since in the grafts the rosettes were formed with inner/outer segments inward and outer plexiform layer side outward, basically in the correct position to form host-graft interaction, we roughly measured the percentages of the rosette area that can possibly contact host INL (the presence of graft ONL approximately within 10 μm from host retinal margin) (Figure S2E). We estimated that graft photoreceptors of approximately 50.8% ± 7.8% (mean ± SEM, n = 5) of the total graft area may have access to host retina to form synapses.

Light-Responsive Behavior Analyzed by Shuttle-Avoidance System

Because we could not obtain convincing results by optokinetic analysis, on the assumption that, with a small piece of graft in the whole retinal area, these mice may see a very small, spot-like light in some part of their visual field at their best, we adapted a shuttle-avoidance system (SAS)

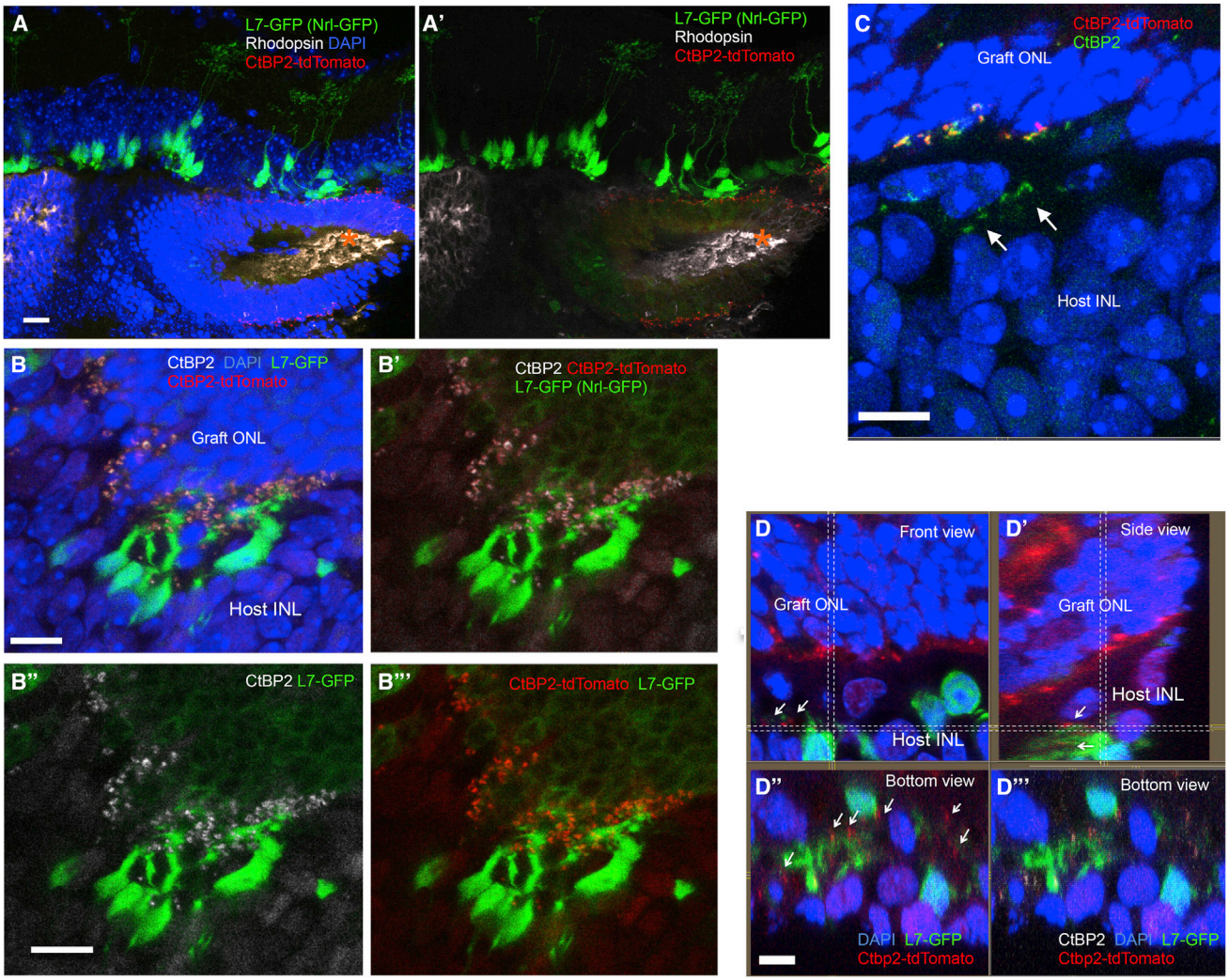

Figure 1. Maturation of Nrl-GFP/ROSA::Nrl-CtBP2-tdTomato Graft Retina

(A and A′) Nrl-GFP/ROSA::Nrl-CtBP2-tdTomato lines formed rhodopsin-positive ONL structures with outer-structure-like segments (asterisk) at DD35 after subretinal transplantation in *rd1* mice, with (A) or without (A′) DAPI nuclear staining (transplanted at DD13). (B–B‴) tdTomato colocalized with anti-CtBP2 immunolabeling at the synaptic terminal of graft photoreceptors (DD35) (B). Merged images with and without DAPI (B, B′) of CtBP2 immunostaining (B″) and CtBP2-tdTomato visualization (B‴) with L7-GFP and Nrl-GFP. (C) CtBP2-positive synaptic terminals in the host retina that were negative for CtBP2-tdTomato (arrows).

(D–D‴) tdTomato-positive graft synaptic terminals in the host retina at and around the tips of GFP-positive host bipolar dendrites (arrows); (D′) shows a side view of the sectional plane at the vertical dotted line in (D); (D″) shows a bottom view of the plane at the horizontal dotted line in (D); (D‴) shows CtBP2-tdTomato within the host retina was stained with the anti-CtBP2 antibody.

Scale bars, 20 μm (A, C) and 10 μm (B, D).

(Figures 3A–3C; see also Experimental Procedures for detailed protocols) to test visual function. To detect both rod and cone function to the greatest extent possible, we used a mesopic light stimulus of 0.3 cd/m^2 with dark-adapted mice, and supplied the mice with 9-*cis* retinol acetate in case isomerization of all-*trans* retinol may be inhibited, since the grafted ONLs often form rosettes with their outer segments being separated from the retinal pigment epithelium (RPE). The avoidance ratio is often used as an index (Jiang et al., 1996), but mice tend to move more randomly when they are not confident of avoiding the stimuli, which can increase the avoidance ratio simply by chance. Thus, instead of simply accepting the avoidance rate, we included inter-trial interval (ITI) counts as an additional observation: for every tested animal, we fitted the observed results to a model with three parameters, namely β_1, β_2, and β_3,

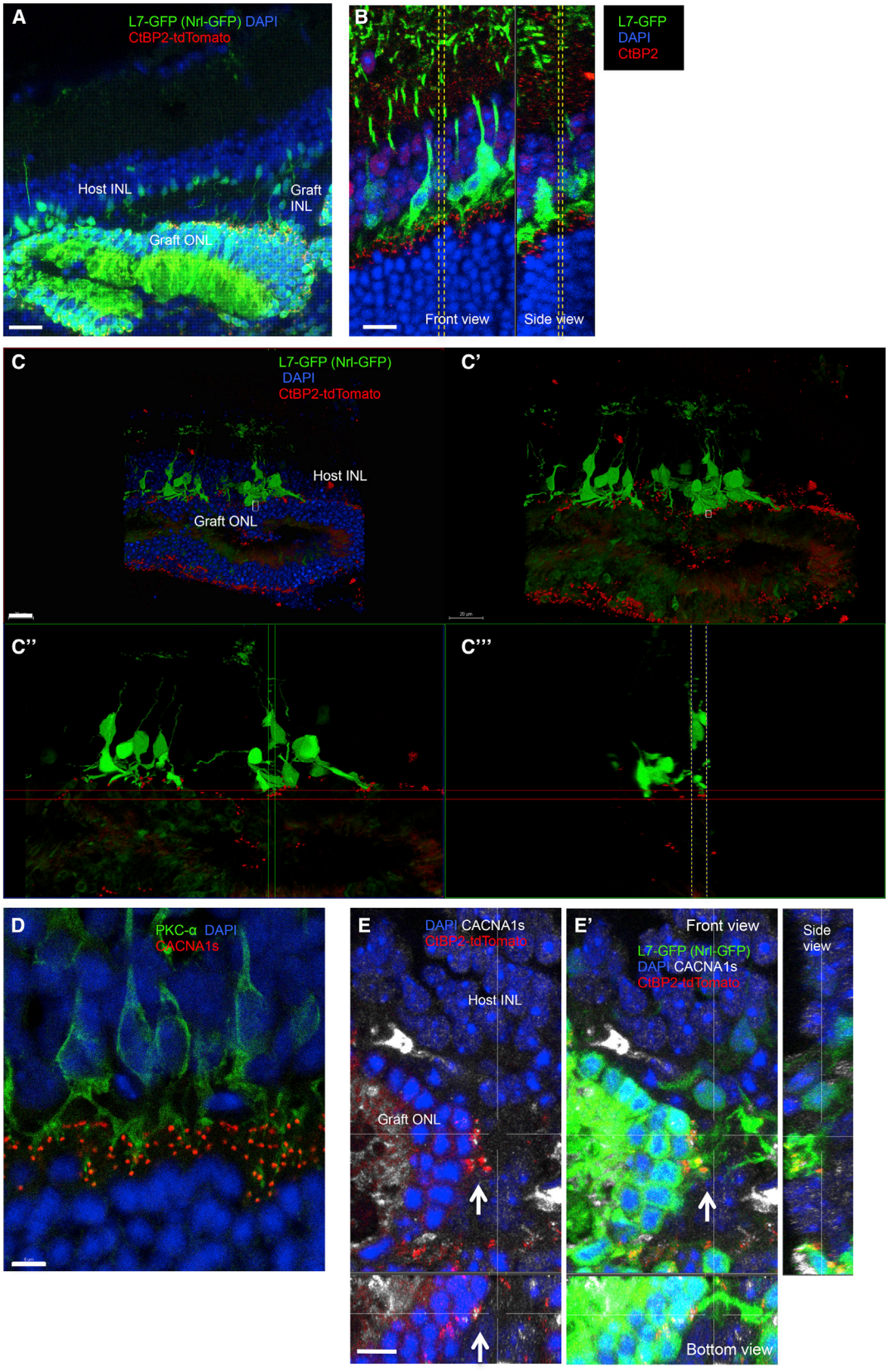

(legend on next page)

and estimated the parameters as features of the animal (Figure S3A). Among these parameters, β_3 showed the effect of interference with visual function. When the 95% credible interval of the distribution of the estimated β_3 was above zero, we judged that interference (mostly transplantation in our study) improved visual function. We included non-treated *rd1* (*rd1/B6*) mice as reference data (n = 11) for comparison with each mouse (Figure 3D, black dots and curves). Another *rd1* strain, *rd1-2J*, was also tested on this system to check the reliability of the SAS test, and because *rd1-2J* were also used in multiple-electrode array (MEA) analysis. When mice were given simultaneous light and audio (beep) signals, the wild-type and *rd1-2J* mice had similarly high success ratios and low ITIs (Figures S3B and S3C). However, when we switched to a light-only signal, the wild-type mice quickly learned to respond whereas *rd1-2J* mice did not, with or without 9-*cis* retinol acetate treatment, much like *rd1/B6* mice (Figures 3D and 3E). We then tested the rd1 mice with good iPSC-retina transplants by OCT (Figure S3D). After retinal transplantation, 4 of 10 mice with transplants in both eyes (B) and 5 of 11 mice with a transplant in only one eye (M) were judged to have responded to the light signal (Figures 3F and 3G) while none of the eyes with poor grafting (graft leakage in the vitreous space or retinal detachment in *rd1/B6*) responded to light. Typical data for a light-responsive grafted mouse and for one with no response are shown in Figure 3H; the light-signal tests are shown in Movies S1 and S2 (for M10 and M8, respectively).

mERG and RGC Recordings from Transplanted Host *rd1* Retinas

Next, we used a multielectrode arrays (MEA) system to analyze mERG and RGC recordings. We previously found that mERG in the wild-type retina shows the a- and b-wave-like component similar to the full-field ERG, and the mERG responses were well correlated with responses by RGCs (Fujii et al., 2016). In the wild-type retina, the b-wave that typically represents ON bipolar cell response as well as RGC ON response disappears by the use of mGluR6 receptor agonist L-AP4, whereas in *rd1-2J* mice, mERG responses were detected only up to 5 weeks old and all the wave components were abolished by L-AP4, indicating the modified intra-retinal signal transmission in these mice (Fujii et al., 2016). In the present study, we transplanted iPSC retinas into *rd1* mice at 7 or more weeks of age, and tested their responses by MEA 1.5–4 months later. We analyzed seven retinas after transplantation. The host mouse lines, ages, graft-source iPSC lines and clones, and time after transplantation are summarized in Table 1, along with the number of electrodes on the grafted area and the recorded mERG or RGC responses. The number of RGC responses was objectively calculated followed by the spike sorting and clustering of spike patterns as described in Experimental Procedures and Figures S5A and S5B. We detected mERGs only from the grafted area in all of the samples tested, and representative data are shown in Figures 4A and S4A. The a- and b-wave amplitudes were generally much smaller than those of wild-type retina and grafted retina sometimes elicited irregular mERG wave patterns, but the positive wave (b-wave) was more frequently observed compared with those of young *rd1-2J* retina (Fujii et al., 2016). The pharmacologic features of mERG and RGC recordings on the representative channels are also shown from the samples TP-5 (Figures 4A–4D), TP-4, and TP-6 (Figure S4B). Typical a- and b-waves were recorded on channels 15 and 16 (thick graft area), whereas only b-waves were recorded on channels 25 and 26 (graft margins) (Figure 4A). L-AP4 treatment abolished the b-waves (black arrows in Figures 4C and S4B) in both cases, in association with the elimination of transient ON RGC responses (blue arrows in Figures 4D and S4B), similar to the responses in wild-type retina in mERG (Figure 4E), indicating that light-responsive signals were transmitted to ON bipolar cells and then to host RGCs in the grafted area.

Clustering RGC Light Responses in the Host *rd1* Retina after Transplantation

We also adapted deep-learning methods to cluster the RGC spike patterns into groups that included both ON

Figure 2. Synaptic Integration of Nrl-GFP/ROSA::Nrl-CtBP2-tdTomato Graft Retina into L7-GFP Host Mice

(A) GFP-positive bipolar cells extend their dendrites through graft INL to reach CtBP2-tdTomato on graft ONL (DD78).

(B) CtBP2-positive presynaptic terminals contact the tips of rod bipolar dendrite terminals in L7-GFP wild-type retina. Front view image of the section between the yellow dashed lines in side view, and side view image of the section between the yellow dashed lines in front view are presented.

(C–C‴) 3D observation of contact between GFP-positive host bipolar cells and CtBP2-tdTomato in the graft ONL (DD35) with (C′) and without (C) DAPI nuclear stainings, with front (C″) and side slice views (C‴). (C″) is the image of the section between the yellow dashed lines in (C‴), and (C‴) is the image of the section between the two vertical lines in (C″).

(D) CACNA1s localizes at dendritic tips of PKCα-positive dendrite terminals in a wild-type retina.

(E and E′) CtBP2-tdTomato in the graft ONL (DD78) are coupled with CACNA1s (arrows) at the tips of L7-GFP-positive host bipolar cells as shown in the side and bottom sliced views.

Scale bars, 20 μm (A, C), 10 μm (B), and 5 μm (D, E).

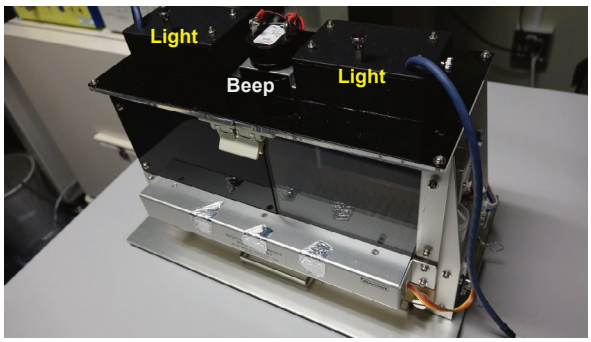

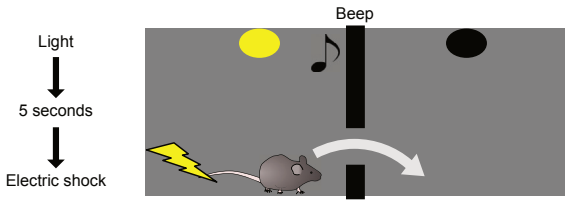

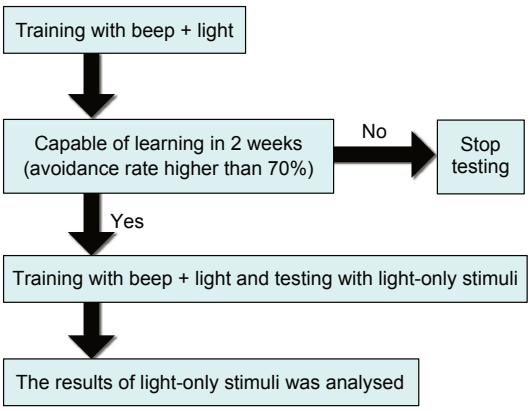

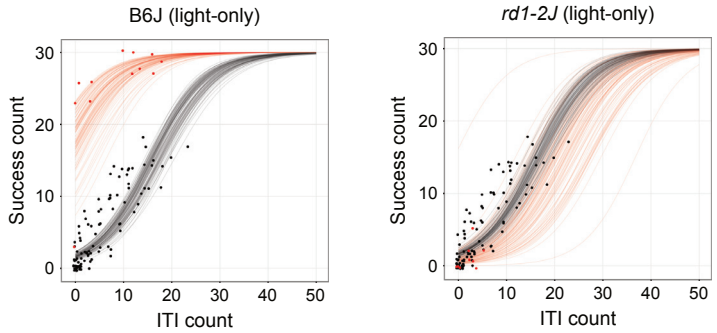

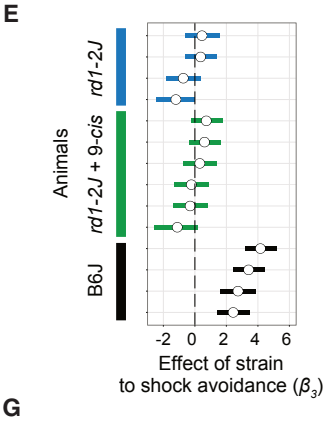

	Graft+		No grafts
	Bilateral (B)	Monolateral (M)	Unsuccessful (N)
Total eyes	10	11	9
Positive response	4 (40%)	5 (45%)	0

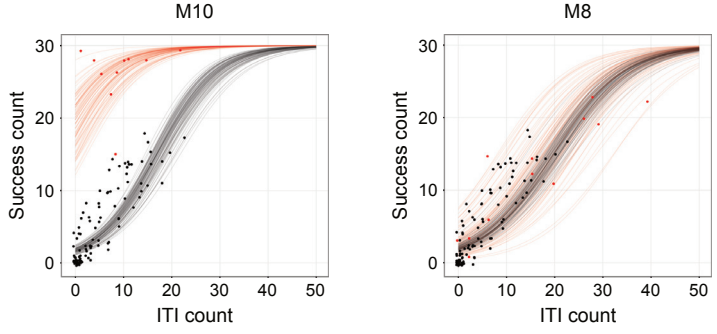

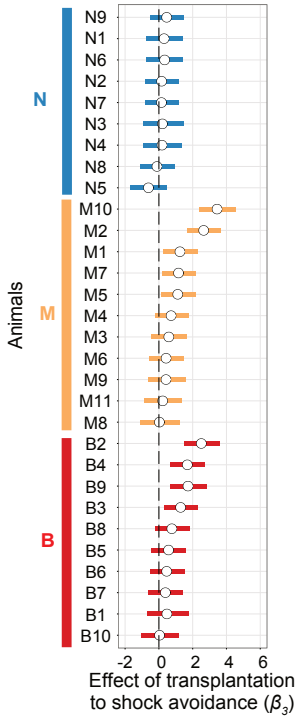

(legend on next page)

Table 1. Summary of Each Retina Sample Used for MEA Analysis

Sample	Host	Host Age (Weeks)	Graft Cell Line	Graft Age	Post-TP (Months)	No. of Electrodes			No. of Spike Sources (RGCs)
						On the Graft	With mERG	With RGC Responses	
TP-1	*rd1/B6*	8	Nrl-GFP	DD14	3	19	4	3	5
TP-2	*rd1-2J*	9	Nrl-GFP	DD14	4	15	8	5	6
TP-3	*rd1-2J*	7	Nrl-GFP	DD13	2	9	8	1	1
TP-4	L7-GFP/*rd1*	8	Nrl-GFP/ROSA::Nrl-CtBP2-tdTomato#1	DD13	1.5	15	12	3	8
TP-5	L7-GFP/*rd1*	8	Nrl-GFP/ROSA::Nrl-CtBP2-tdTomato#2	DD13	2	43	58	49	112
TP-6	L7-GFP/*rd1*	8	Nrl-GFP/ROSA::Nrl-CtBP2-tdTomato#2	DD13	2	51	44	10	17
TP-7	L7-GFP/*rd1*	8	Nrl-GFP/ROSA::Nrl-CtBP2-tdTomato#3	DD13	2	8	6	0	0

The following information was provided for each tested retina. The host age/graft age in differentiation days (DD) at the time of transplant; the number of months of post-transplant (TP) MEA recordings; the number of electrodes present; the number of electrodes on the grafted area, those positive for mERG recordings, and those positive for RGC responses; and the number of spike sources (RGCs) that were categorized in a cluster other than the non-specific pattern.

and OFF responses (Figures 5A and 5B). Transient ON, OFF, and ON-OFF responses were most dominant in the wild-type (B6) retina with a full-field light flash of 0.45 log cd/m^2; these shifted to a transient OFF response when mGluR6 was blocked (Figure 5A). In retinas from 7-week-old or older *rd1-2J* mice, all of the spikes were clustered as non-specific patterns except for 0.2% of the ON-hyperactive pattern. However, we detected transient ON responses consistently in the grafted area, with an average of 5% (0% to 16% at maximum) of all the detected RGC sources from the whole recorded area (Figure 5A). The number of detected response sources (RGCs) and their patterns are shown for each tested retina in Figure 5B. Generally the grafts that covered a larger number of electrodes elicited a higher number of RGC responses, whereas in the samples where grafts were placed on a small number of electrodes in the experimental setting (TP-3 and TP-7, with 9 and 8 electrodes, respectively) only few or no typical RGC responses were recorded (Table 1). When the number of typical light responses (transient ON/transient OFF/ON-OFF) was plotted against the number of electrodes with graft, it showed a linear correlation tendency except for TP-5, which showed an exceptionally good result among the tested samples (Figure 5C). These RGC responses over the graft were clearly distinguishable from residual RGC activity in the degenerating *rd1* retina; *rd1* retina elicited either a non-specific pattern with regular intensity stimuli, or hyperactive patterns (ON, OFF, and delayed) shown as clustering groups mostly with higher-intensity stimuli (3.01 log cd/m^2) as in the training dataset (Figure S5A).

Figure 3. Shuttle-Avoidance Behavioral Tests in *rd1* Mice with Retinal Transplants

(A) The shuttle box has two compartments, a light in each compartment, and a beeping device in the middle.

(B) An electric shock is delivered after 5 s of continuous light with or without beeping.

(C) The experimental protocol for shuttle-avoidance testing (see Experimental Procedures).

(D) Representative results for shuttle-avoidance tests using only light signaling for a wild-type (B6) mouse (left) and an *rd1* (*rd1-2J*) mouse (right). The behavior of the wild-type mouse deviated significantly from that of an untreated control *rd1* mouse, while that of the *rd1* (*rd1-2J*) mouse did not. Dots denote the observed SAS test results (see also H) and the lines are estimated relationships of ITI count and SAS success count (30 trials in total) simulated from randomly selected posterior samples of the model; black and red indicate the control and the subject, respectively.

(E) Posterior distributions of the estimated effect of strain difference or 9-*cis* retinol acetate administration to shock avoidance for *rd1-2J* and wild-type mice. White circles denote the median; bars denote the 95% confidence interval (CI) of the posterior distribution of β_3 for each animal (see also G). The 95% CI of all wild-type mice was above zero.

(F) The number of mice that behaved differently from control *rd1* mice in three groups: those with unsuccessful transplantation (N), a retinal transplant in one eye (M), and transplants in both eyes (B).

(G) Posterior distributions of the estimated effect of transplantation to shock avoidance (β_3) for all mice that underwent SAS tests.

(H) Representative SAS test results for individual mice (M8 and M10) with retinal transplants, with positive and negative results.

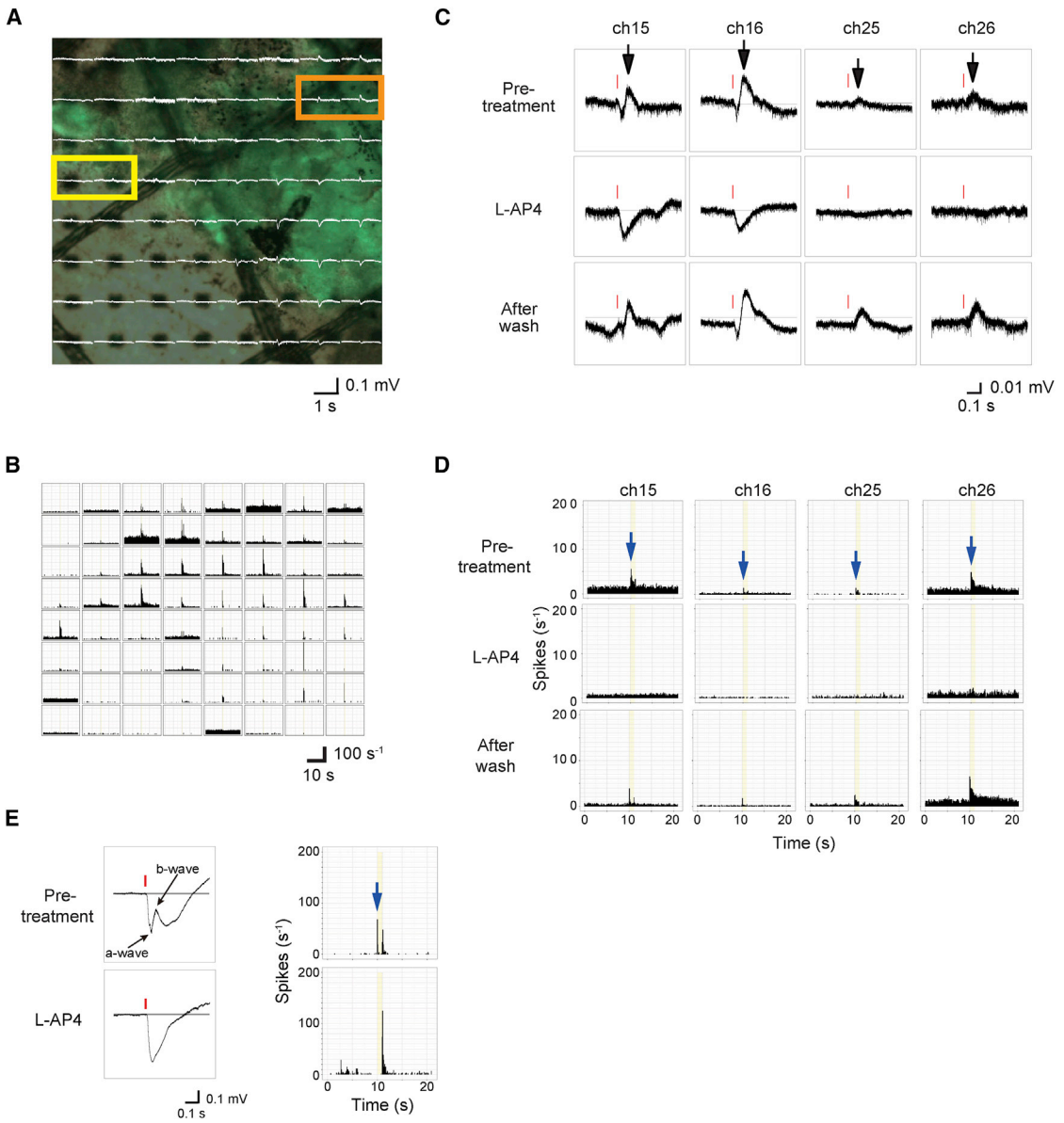

Figure 4. Ex Vivo MEA mERG and RGC Recordings from Transplanted Retinas

(A) mERGs overlaid on a photograph of the isolated retina (TP-5 in Table 1) on the MEA microelectrodes.

(B) RGC responses on each electrode in histograms after spike sorting.

(C and D) Representative mERG (C) and RGC responses (D) in channels 15, 16 (orange box in A where the graft is thick), 25, and 26 (yellow box in A at graft margin) with or without the mGluR6 blocker. Black arrows indicate b-waves and red lines indicate timing of the signal flash (C). Blue arrows indicate transient ON responses and yellow bands indicate the timing and the duration of light stimuli (D).

(E) A typical mERG wave pattern and RGC responses of a wild-type retina before and after L-AP4 treatment. After treatment of L-AP4, the b-wave in mERG and ON response (blue arrow) in RGC recording disappears.

3D Image Reconstruction of the Samples after MEA Recordings

To eliminate the possibility of a contaminant response from graft cells, we reconstructed 3D histological images of the MEA-recorded area after MEA analysis and carefully observed host-graft integration over the MEA-recorded channels (Figures 6A–6C). The sectional views over the channels presented in Figure 4D (channels 16 and 25) revealed that the Nrl-GFP-positive graft ONLs expressed the presynaptic marker CtBP2-tdTomato at the host-graft interfaces (red arrows) in contact with the host INLs (white arrows), which contained L7-GFP-positive bipolar

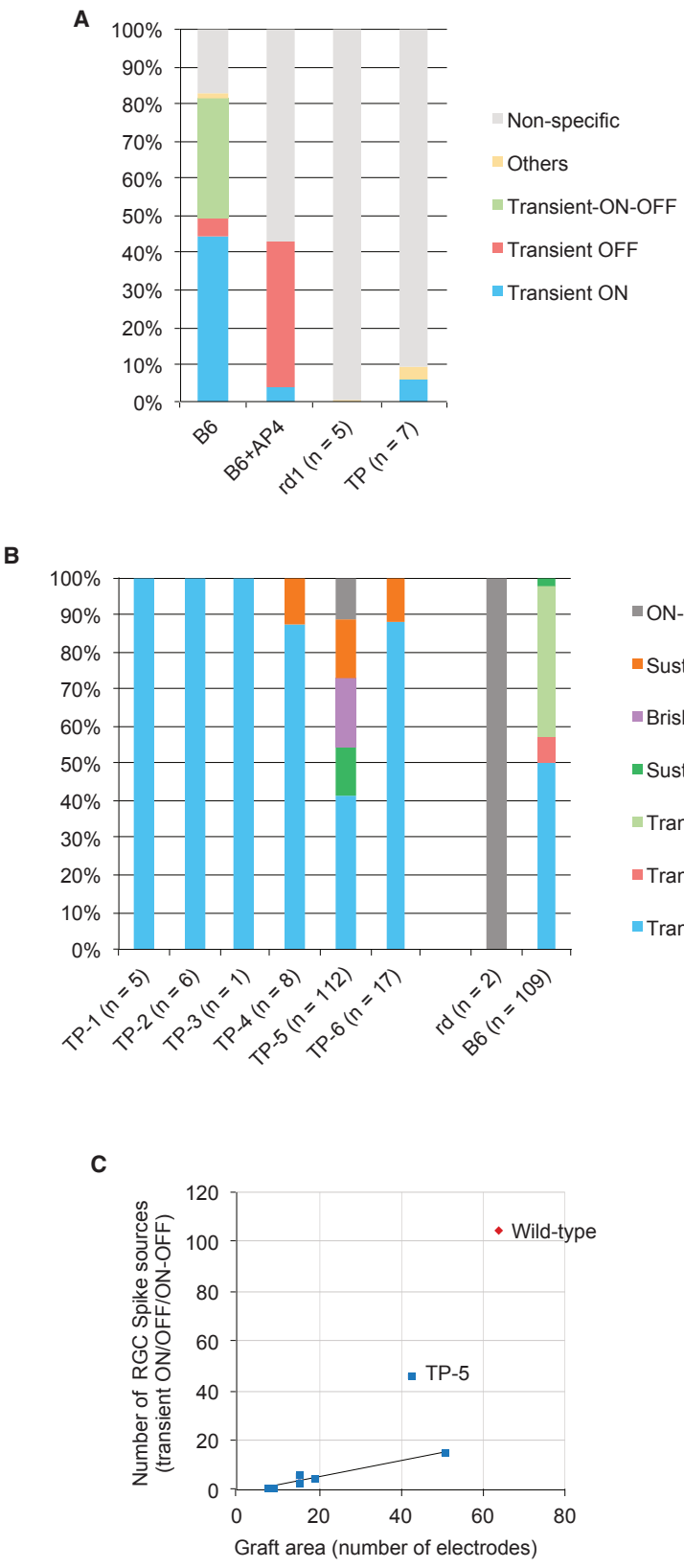

Figure 5. Quantitative Analysis on RGC Spike Sources after Transplantation

(A) RGC spike patterns among all of the detected spike sources in wild-type retinas (n = 2 retinas) with or without mGluR6 blocker, and in *rd1* retinas with (n = 7) or without (n = 5) iPSC-retina transplants.

(B) Details of RGC spike patterns in each retina sample after transplantation, clustered into each pattern shown in Figure S5A. Sample TP-7 is not shown because no spike source was clustered into any specific group. The number of detected spike sources is shown below each retina.

(C) Number of RGC sources with typical light-responsive spikes in wild-type retina (transient ON/OFF and ON-OFF in Figure S5A) are plotted against the graft area indicated as the number of electrodes on x axis.

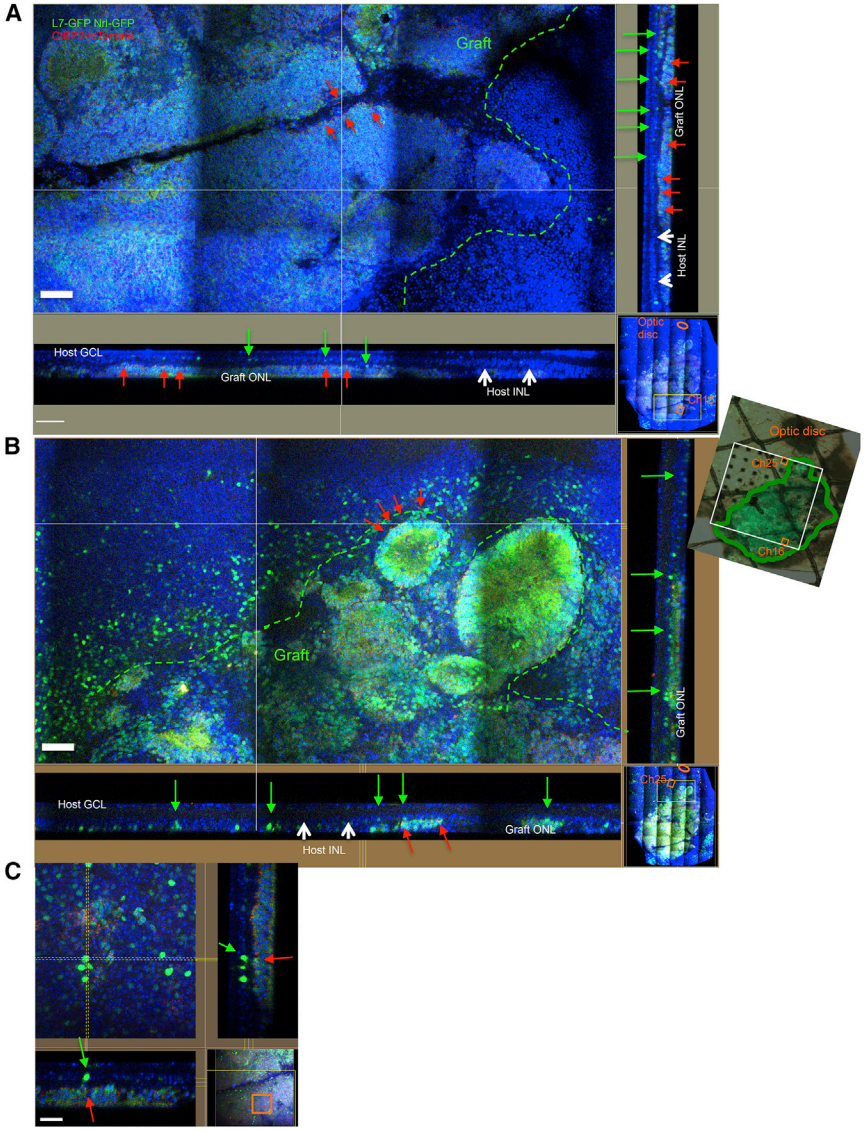

Figure 6. 3D Histological Analysis of Retinal Transplants after MEA Recordings
Tiled images of the retina after MEA (sample 5 in Table 1). The area on electrode channels 16 (A) and 25 (B) (orange box on MEA photograph) are shown with vertical section views. Green dotted lines indicate graft margin on the electrodes. Orange ovals indicate optic discs. Green arrows indicate L7-GFP-positive host bipolar cells in host INL (white arrows). CtBP2-tdTomato-positive graft synaptic terminals are present on the graft ONL margin (red arrows). (C) Magnified view of the section close to (A). Scale bars, 50 μm (A, B) and 20 μm (C).

cells (green arrows). Channel 16 showed larger, thicker graft ONL than those observed in channel 25, consistent with the presence of marked a-waves on channel 16 but not channel 25 (Figure 4C).

DISCUSSION

We have previously shown that retinal tissues differentiated from mouse or human ESCs or iPSCs could develop to form ONLs consisting of mature photoreceptors with highly differentiated structures such as inner/outer segments after transplantation in the degenerated host retina (Assawachananont et al., 2014; Shirai et al., 2015). We also showed that these graft ONL integrated as a structured layer to the host inner layers possibly with host-graft synaptogenesis. However, the functional evaluation was yet to be performed.

In the current study, with the use of Nrl-GFP/CtBP2-tdTomato cell lines with host L7-GFP/*rd1* mice, we readily visualized direct contact between the host-graft cells, and our observations revealed that host bipolar cells extend their dendrites into the graft, sometimes even through the remaining graft inner cells (Figure 1C). Retraction of bipolar cell dendrites were observed after photoreceptor degeneration (Marc et al., 2003), and transplanted photoreceptors seem to provide some environmental change for the host bipolar cells to regrow dendrites. The reason for and effect of the variable degree of host L7-GFP expression in PKCα-positive rod bipolar cells with *rd1* phenotype is not known, but the use of the present host-graft combination may further help to quantitatively access the host-

graft integration in our future studies in optimizing the transplantation conditions.

To evaluate visual function through behavioral tests, we first tried optokinetic testing (OKT). Some of the mice with retinal transplants did not noticeably track the moving bars but became exceptionally static. Considering the relatively small graft area and the unknown efficiency of synaptogenesis, these mice probably saw a very small, spot-like light in some part of their visual field. We concluded that OKT was inadequate for detecting visual function in these mice. In addition, OKT has shown conflicting results in retinal degeneration and should be used with caution (McGill et al., 2012). Likewise, these transplanted mice will not follow regular light-avoidance behavior patterns if they only see small or ambient light. This led us to adapt SAS for objective evaluation of their behavior patterns in response to light. The SAS requires approximately 2 weeks of training with beep and light, and 2 more weeks of evaluation with a light-only signal, so we restricted the use of analysis to only the mice with a substantial amount of subretinal graft as judged by in vivo OCT imaging after transplantation. There was no difference in the results between mice with transplants in one or both eyes, and we assume that the graft area, and possibly the location, may contribute to the sensitivity of visual perception in our SAS evaluation.

For the photoreceptors to function, recycling of visual pigments by isomerization and oxidation, from all-*trans* retinol to 11-*cis* retinol, and to 11-*cis* retinal, is essential (Parker and Crouch, 2010). The first essential step of isomerization to form 11-*cis* retinol is catalyzed by RPE65 in RPE for rod visual pigments (Redmond et al., 1998) and in Muller cells for cone visual pigments (Travis et al., 2005). The further oxidation to restore 11-*cis* retinal is then catalyzed by retinol dehydrogenases (RDHs), which are distributed in retina and RPE in a number of isoforms with overlapping activities (Maeda et al., 2007; Parker and Crouch, 2010). Because the grafted ONLs often form rosettes with their outer segments being separated from the RPE, isomerization of all-*trans* retinol may be inhibited. Since the treatment of 9-*cis* retinyl acetate (9-*cis* retinol acetate) restored the impaired visual function in *Rpe65*$^{-/-}$ mice (Maeda et al., 2009), we supplied 9-*cis* retinol acetate when we performed a behavior test with light-only signals to supply a substantial amount of the source of 11-*cis* retinal, although not the direct competent form. Partly because SAS was a time-consuming test, we did not perform the experiments with or without the drug treatment, or the tests after washout, so we were unable to determine the effects of 9-*cis* retinol acetate supplementation. Treatment of 9-*cis* retinol acetate had no effect on unsuccessful transplantation or non-treated rd1 mice, so the change in SAS results after transplantation is not due to the protective effect by the treatment.

In electrophysiological evaluation using MEA, we carefully evaluated the graft-originated responses not simply by their presence or absence but by their functional properties. The presence of mERG responses were hardly detected in *rd1* host retinas at 7 weeks or older, and, even in earlier degeneration, all the wave components were eliminated by mGluR6 blockade by L-AP4 (Fujii et al., 2016). After transplantation, marked light-responsive mERGs were recorded in the grafted area in all the samples tested, although the amplitudes were smaller than those of wild-type retina and the wave patterns were more variable, indicating that graft is responsive to light. The presence of the remaining negative-wave components after mGluR6 blockade implies that these responses may originate either from the graft photoreceptors or OFF components of host second neurons, which were both absent in *rd1* host retinas before transplantation (Fujii et al., 2016). Furthermore, we were able to record significant light-responsive spikes from the host RGC layer, most of which were clustered as transient ON patterns. With our MEA system, approximately 20 cells are on one electrode in the RGC layer, half of which are reportedly amacrine cells (Jeon et al., 1998). Possible flaws in interpreting these RGC recordings include (1) residual responses from the host (cone) photoreceptors, (2) light-dependent RGC responses from intrinsically photosensitive retinal ganglion cells (iRGCs) (Berson et al., 2002; Hattar et al., 2002; Pickard and Sollars, 2012), and (3) spikes from graft cells, including graft RGCs, that may have been exposed on the host RGC surface layer. As we have described, the possibility of residual host transient ON function is unlikely. The possibility of iRGC activities can also be discounted, because the L-AP4 blockage of mGluR6 demonstrated that the RGC responses were postsynaptic. We also observed that in the area where light-responsive RGCs were recorded, the RGC and inner layers of host retina was present by histological examination, leaving little possibility that these RGC responses were mostly contributed by exposed graft cells. Interestingly, the channels that elicit RGC responses and those with evident mERG responses are not completely the same, such as seen in TP-6 in Figure S4A, which indicated that the former may represent the graft status such as the presence of graft photoreceptor outer segments in correct orientation, whereas the latter may represent the location of RGCs that eventually received input from graft light response. A few RGC responses detected outside the graft margin, as shown in Figure 4B, may also support that the responses derive from the host RGCs that may include the graft area in their receptive fields.

This proof-of-concept study showed that the iPSC retina, when transplanted into the eyes of end-stage

retinal-degeneration mice, develops a mature ONL and responds to light. Nearly half of the mice with retinal transplant showed light-responsive behavior. We recently showed that the hESC retina can develop and mature after being transplanted into the eyes of monkeys with ONL-lost retinal degeneration (Shirai et al., 2015). We are currently testing the competency of a human iPSC retina to restore visual function.

EXPERIMENTAL PROCEDURES

All animal experiments were conducted in accordance with local guidelines and the ARVO statement on the use of animals in ophthalmic and vision research. All of the experimental protocols were approved by the committee of the RIKEN Center for Developmental Biology (CDB).

Animals

The mouse lines *rd1-2J* and Tg(Pcp2-EGFP)2Yuza were obtained from The Jackson Laboratory and C3H/Hej Yok Slc strain mice were obtained from Nihon SLC (Shizuoka, Japan). Tg(Pcp2-EGFP)2Yuza/*rd1-2J* (L7-GFP/*rd1*) mice were prepared by crossbreeding and establishing homologous transgene-positive *rd1-2J* lines. The *rd1* (*rd1*/*B6*) line was prepared by backcrossing C3H/Hej mice with C57BL/6JJmsSlc mice for several generations. All mice were kept on a standard 12:12-hr light/dark cycle. During behavior tests, the animals were kept in the dark for 24 hr to adapt to darkness. For anesthesia, mice were anesthetized with ketamine hydrochloride (1 mg/10 g weight; Ketalar, Daiichi Sankyo Propharma) and xylazine (0.04%/10 g weight; Selactar, Bayer Yakuhin), and the pupils were dilated using tropicamide and phenylephrine hydrochloride (Midorin-P, Santen Pharmaceutical).

Generation of Nrl-GFP::pNrl-CtBP2-tdTomato Lines

For labeling of synapses, the CtBP2-tdTomato fusion sequence under the *Nrl* promoter was knocked in, in reverse position, into the genome ROSA locus of the Nrl-GFP miPSC line, which was generated from Nrl-eGFP mice (Akimoto et al., 2006; Homma et al., 2013). The targeting method is summarized in Figure S1A and details are described in Supplemental Experimental Procedures.

Differentiation of miPSC Retina and Its Subretinal Transplantation

Nrl-GFP transgenic miPSCs were generated from Nrl-eGFP mice (Akimoto et al., 2006; Homma et al., 2013), and the genetically modified lines were maintained and differentiated as already described (Assawachananont et al., 2014). More details are described in Supplemental Experimental Procedures.

In Vivo OCT Imaging after Transplantation

To confirm that the graft was substantially and properly located in the subretinal space, we obtained SD-OCT (spectral domain ophthalmic imaging system) images with an Envisu R-series SDOIS (Bioptogen) 2–4 weeks after transplantation under anesthesia.

Shuttle-Avoidance System Tests

The shuttle-avoidance system (CompACT SAS/W, Muromachi Kikai) was customized for mesopic testing and placed in a sound- and light-insulated box. The training/test box consisted of two chambers separated by a dark wall with a small opening that allowed the animal to move freely between the compartments (Figures 3A and 3B). The basic concept of this study is to evaluate whether a mouse can learn to avoid the electric shock by moving into the other chamber by the visual perception of light as a warning signal.

The mouse was placed in the box and trained with simultaneous beep and mesopic light (0.3 cd) signals as a pre-warning for an electric shock delivered 5 s later on the floor bars. The mouse could avoid the shock by moving to the other chamber, in which case the trial was considered successful. If the mouse remained in the same chamber and was shocked, the trial was recorded as a failure. One series of training or experiments consisted of 30 trials, each recorded as either successful avoidance or a failure. The signals were given at random intervals. The number of times the mouse moved between the two chambers in the intervals between trials, recorded as ITI counts, was also used as a parameter for analysis. Mice that learned and improved within the first 10 days of SAS training (using both beep and light signals) were used in further experiments. Once the mouse attained a success ratio greater than 70% with simultaneous beep/light signals, the experiment was performed using only a light signal. In the transplanted group, 6- to 9-week-old *rd1*/*B6* mice were subretinally transplanted with iPSC retina of DD11-17 iPSC retina, and SAS training was started at 5 weeks or later after transplantation. Transplanted animals were given an intraperitoneal treatment of 9-*cis* retinol acetate (0.0125 mg/mouse/day; Toronto Research Chemicals) for 4 days each week during the SAS period to supply a substantial amount of the source of 11-*cis* retinal in case graft ONL were not in contact with RPE. Experiments using only light signals were performed only after the mouse had passed the dual beep/light-signal test on the same day. Success ratios and ITI counts using only the light signal were recorded for each mouse until the response of the mouse appeared to plateau. Training and experiments were performed daily except for weekends, with either one series (beep/light) or two series (beep/light followed by light only) per day.

Analysis of the Shuttle-Avoidance Test

To evaluate shuttle-avoidance test results as an index for visual perception of light, we constructed a binomial generalized linear mixed model, in which the success rate is described as a function of ITI count and the retinal implantation state of the animal. Estimating the parameters of the model by Markov Chain Monte Carlo (MCMC) sampling using Stan (Stan Development Team, 2016a) (version 2.10.1) with the RStan library (Stan Development Team, 2016b) (version 2.10.1) in R (R Core Team, 2015) (version 3.3.0), we tested whether visual acuity had improved in each retina-grafted mouse based on the posterior distribution of the estimated parameters.

First, we assumed that the count for successful avoidance y_i within 30 SAS trials, counted on the i^{th} test, followed a binomial distribution for the probability q_i, which is the avoidance

probability of a single SAS trial during the i^{th} test. Thus, y_i can be described as

$$y_i \sim \text{Binomial}(q_i),$$
$$p(y_i|N, q_i) = \binom{N}{y_i} q_i^{y_i} (1-q_i)^{N-y_i},$$
$$0 \le y_i \le N,$$
$$N = 30.$$

Second, we described the probability q_i as a function of ITI count, the retinal implantation state, and the random effect of an individual mouse. The explanatory variables included a continuous fixed effect x_i for ITI counts of the i^{th} test, a categorical fixed effect f_j for retinal implantation, and individual random effects r_j of the j^{th} mouse; r_j was described with a normal distributions with a mean of zero and variance σ_j. Applying the logistic transformation, q_i can be described as

$$q_i = \frac{1}{1+\exp(-z_i)}$$
$$z_i = \beta_1 + \beta_2 x_i + \beta_3 f_j + r_j$$
$$f_j \sim \begin{cases} 0, \text{ when no retina was transplanted} \\ 1, \text{ when retina was transplanted} \end{cases},$$
$$r_j \sim \text{Normal}\left(0, \sigma_j^2\right)$$

where β_1, β_2, and β_3 denote coefficients of the linear predictor z_i. β_1 is the base coefficient, which is common among every SAS test included in the analysis. In other words, this coefficient describes the q_i when ITI count is zero with no interference. β_2 is the coefficient for x_i, which shows how the ITI count affects the shock avoidance rate. This should be positive because if ITI count increases, the rate for the animal to avoid shock by chance should increase. β_3 is the coefficient showing the effect of interference to shock avoidance. In this study, retinal transplantation was mostly the interference. If β_3 is positive, the interference is estimated to increase the q_i. For each animal with a retinal transplant, this model was fitted by SAS results using the negative-control *rd1* mouse line, which was backcrossed from C3H/HeJ mice with C57BL/6JJmsSlc (*rd1/B6*) mice (n = 11). We judged that the animal's visual function improved when the 95% credible interval of the posterior distribution of β_3 was above zero. Moreover, any type of interference can be tested if it is provided as f_i. Therefore, to test the functionality of this method, we estimated the β_3 for wild-type animals or another group of *rd* mice (Figure 3D). The estimated β_2 was constantly positive, indicating that the larger the ITI count, the larger the q_i. Uniform priors were applied for every estimated parameter for MCMC sampling.

Classification of Light Responses by Deep-Learning Models

The deep-learning model for classifying light responses was built on an open-source machine-learning platform H2O (version 3.8.2.6) (www.h2o.ai) accessed from R (R Core Team, 2015) (version 3.3.0). First, a manually classified light-response dataset (Data S1) was prepared for training and validating the model. The annotated training dataset used in this study is available in Data S2 and the light-response binary data can be downloaded at https://goo.gl/JtQqIF (training_data.xdr). Three thousand light responses randomly selected from two wild-type retinas and five *rd1-2J* retinas (7w–38w) using 1 s of 0.45 log cd/m^2 and 3.01 log cd/m^2 light stimuli were classified into 11 clusters based on the response pattern. Cluster 1 was designated as a non-specific response, and the following 10 clusters were designated as functional light responses (Figure S4A). Next, applying the training dataset, we trained two deep-learning models (models 1 and 2) to cluster the light responses. Because more than 85% of the recorded spikes turned out to be cluster 1, model 1 aimed to distinguish between cluster 1 and non-1 clusters. Model 2 was designed to cluster the non-1 responses into clusters 2 to 11. Each light response had 20 s of recordings for 2,000 points of spike frequency within a 0.01-s bin. We fed the deep-learning model with these time series of spiking frequency and with four additional calculated features: the SDs of before and after the light stimuli, and the mean spiking frequency difference around the beginning and the end of the light stimuli (see Data S3 for the detailed calculation formula). We tested several structures for the deep neural network and chose the models with the highest accuracy. For the detailed model structures, please refer to the source code for training (Data S3). In short, model 1 had 2,004 inputs and two outputs, with four hidden layers with 128 inputs. Model 2 had 2,004 inputs and 11 outputs, with five hidden layers with 128 inputs. Every light response in this study was clustered according to the following rules (Figure S4B): the response was classified as cluster 1 when the model 1 was judged so at a confidence level higher than 99.5%, and the remaining (non-1) responses were clustered based on the results of classification by model 2. The source code and the two models can be downloaded at https://goo.gl/dTUv1m (clustering.zip) with sample data. In this study, a single train of spikes had three serial light responses (See MEA Recordings). The majority rule was adopted; thus, when more than two out of three responses were classified into an identical cluster, the cell was classified to the major cluster, and when not was classified as "not classified (N.C.)".

RGC counts were calculated as the sum of before the treatment of and after the washout of L-AP4 on each channel, because sometimes the RGC spikes were more evident on either of these two conditions than the other in a few channels.

MEA Recordings

MEA recordings were performed as previously described (Fujii et al., 2016). Details are included in Supplemental Experimental Procedures.

Immunostaining and 3D Image Reconstruction

Methods for immunostaining and 3D image reconstruction were previously described (Assawachananont et al., 2014). Information for antibodies is included in Supplemental Experimental Procedures.

SUPPLEMENTAL INFORMATION

Supplemental Information includes Supplemental Experimental Procedures, five figures, three data files, and two movies and can be found with this article online at http://dx.doi.org/10.1016/j.stemcr.2016.12.008.

AUTHOR CONTRIBUTIONS

M.M. and M.T. designed and supervised the study. T.H. prepared the KI construct and produced the Nrl-GFP::pNrl-CtBP2-tdTomato lines. T.H., S.I., and J.S. performed cell differentiation. M.M. performed transplantation of the differentiated neural retina and the 3D image analysis. G.A.S. developed the method for clustering the MEA recordings and the method for SAS test evaluation. J.K. and M.F. set up the MEA system. M.F. performed the MEA experiment and analysis. C.Y and J.S. conducted the SAS experiment and analysis. M.M. and G.A.S. wrote the manuscript. All authors reviewed and approved the final manuscript.

ACKNOWLEDGMENTS

We thank Mototsugu Eiraku, Take Matsuyama, Akishi Onishi, Akiko Maeda, and Tadao Maeda for technical advice and supportive discussion. We also thank Takaya Abe for insightful advice on making knockin cell lines. This study was supported by the Research Center Network for Realization of Regenerative Medicine from the Japan Agency for Medical Research and Development (AMED) (M.T.) and by JSPS KAKENHI grant number 15K10913 (M.M.).

Received: September 7, 2016
Revised: December 7, 2016
Accepted: December 8, 2016
Published: January 10, 2017

REFERENCES

Akimoto, M., Cheng, H., Zhu, D., Brzezinski, J.A., Khanna, R., Filippova, E., Oh, E.C.T., Jing, Y., Linares, J.-L., Brooks, M., et al. (2006). Targeting of GFP to newborn rods by Nrl promoter and temporal expression profiling of flow-sorted photoreceptors. Proc. Natl. Acad. Sci. USA *103*, 3890–3895.

Assawachananont, J., Mandai, M., Okamoto, S., Yamada, C., Eiraku, M., Yonemura, S., Sasai, Y., and Takahashi, M. (2014). Transplantation of embryonic and induced pluripotent stem cell-derived 3D retinal sheets into retinal degenerative mice. Stem Cell Reports *2*, 662–674.

Barnea-Cramer, A.O., Wang, W., Lu, S.-J., Singh, M.S., Luo, C., Huo, H., McClements, M.E., Barnard, A.R., MacLaren, R.E., and Lanza, R. (2016). Function of human pluripotent stem cell-derived photoreceptor progenitors in blind mice. Sci. Rep. *6*, 29784.

Berson, D.M., Dunn, F.A., and Takao, M. (2002). Phototransduction by retinal ganglion cells that set the circadian clock. Science *295*, 1070–1073.

del Cerro, M., Humayun, M.S., Sadda, S.R., Cao, J., Hayashi, N., Green, W.R., del Cerro, C., and de Juan, E. (2000). Histologic correlation of human neural retinal transplantation. Invest. Ophthalmol. Vis. Sci. *41*, 3142–3148.

Fujii, M., Sunagawa, G.A., Kondo, M., Takahashi, M., and Mandai, M. (2016). Evaluation of micro electroretinograms recorded with multiple electrode array to assess focal retinal function. Sci. Rep. *6*, 30719.

Gonzalez-Cordero, A., West, E.L., Pearson, R.A., Duran, Y., Carvalho, L.S., Chu, C.J., Naeem, A., Blackford, S.J.I., Georgiadis, A., Lakowski, J., et al. (2013). Photoreceptor precursors derived from three-dimensional embryonic stem cell cultures integrate and mature within adult degenerate retina. Nat. Biotechnol. *31*, 741–747.

Hasan, N., Ray, T.A., and Gregg, R.G. (2016). CACNA1S expression in mouse retina: novel isoforms and antibody cross-reactivity with GPR179. Vis. Neurosci. *33*, E009.

Hattar, S., Liao, H.W., Takao, M., Berson, D.M., and Yau, K.W. (2002). Melanopsin-containing retinal ganglion cells: architecture, projections, and intrinsic photosensitivity. Science *295*, 1065–1070.

Homma, K., Okamoto, S., Mandai, M., Gotoh, N., Rajasimha, H.K., Chang, Y.S., Chen, S., Li, W., Cogliati, T., Swaroop, A., and Takahashi, M. (2013). Developing rods transplanted into the degenerating retina of Crx-knockout mice exhibit neural activity similar to native photoreceptors. Stem Cells *31*, 1149–1159.

Jeon, C.J., Strettoi, E., and Masland, R.H. (1998). The major cell populations of the mouse retina. J. Neurosci. *18*, 8936–8946.

Jiang, H., Lyubarsky, A., Dodd, R., Vardi, N., Pugh, E., Baylor, D., Simon, M.I., and Wu, D. (1996). Phospholipase C beta 4 is involved in modulating the visual response in mice. Proc. Natl. Acad. Sci. USA *93*, 14598–14601.

Kuwahara, A., Ozone, C., Nakano, T., Saito, K., Eiraku, M., and Sasai, Y. (2015). Generation of a ciliary margin-like stem cell niche from self-organizing human retinal tissue. Nat. Commun. *6*, 6286.

Maeda, A., Maeda, T., Sun, W., Zhang, H., Baehr, W., and Palczewski, K. (2007). Redundant and unique roles of retinol dehydrogenases in the mouse retina. Proc. Natl. Acad. Sci. USA *104*, 19565–19570.

Maeda, T., Maeda, A., Casadesus, G., Palczewski, K., and Margaron, P. (2009). Evaluation of 9-cis-retinyl acetate therapy in Rpe65-/- mice. Invest. Ophthalmol. Vis. Sci. *50*, 4368–4378.

Mandai, M., Homma, K., Okamoto, S., Yamada, C., Nomori, A., and Takahashi, M. (2012). Adequate time window and environmental factors supporting retinal graft cell survival in rd mice. Cell Med. *4*, 45–54.

Marc, R.E., Jones, B.W., Watt, C.B., and Strettoi, E. (2003). Neural remodeling in retinal degeneration. Prog. Retin. Eye Res. *22*, 607–655.

McGill, T.J., Prusky, G.T., Douglas, R.M., Yasumura, D., Matthes, M.T., Lowe, R.J., Duncan, J.L., Yang, H., Ahern, K., Daniello, K.M., et al. (2012). Discordant anatomical, electrophysiological, and visual behavioral profiles of retinal degeneration in rat models of retinal degenerative disease. Invest. Ophthalmol. Vis. Sci. *53*, 6232–6244.

Nakano, T., Ando, S., Takata, N., Kawada, M., Muguruma, K., Sekiguchi, K., Saito, K., Yonemura, S., Eiraku, M., and Sasai, Y. (2012). Self-formation of optic cups and storable stratified neural retina from human ESCs. Cell Stem Cell *10*, 771–785.

Parker, R.O., and Crouch, R.K. (2010). Retinol dehydrogenases (RDHs) in the visual cycle. Exp. Eye Res. *91*, 788–792.

Pearson, R.A., Barber, A.C., Rizzi, M., Hippert, C., Xue, T., West, E.L., Duran, Y., Smith, A.J., Chuang, J.Z., Azam, S.A., et al.

(2012). Restoration of vision after transplantation of photoreceptors. Nature *485*, 99–103.

Pearson, R.A., Gonzalez-Cordero, A., West, E.L., Ribeiro, J.R., Aghaizu, N., Goh, D., Sampson, R.D., Georgiadis, A., Waldron, P.V., Duran, Y., et al. (2016). Donor and host photoreceptors engage in material transfer following transplantation of post-mitotic photoreceptor precursors. Nat. Commun. *7*, 13029.

Pickard, G.E., and Sollars, P.J. (2012). Intrinsically photosensitive retinal ganglion cells. Rev. Physiol. Biochem. Pharmacol. *162*, 59–90.

R Core Team. (2015). R: A Language and Environment for Statistical Computing (R Foundation for Statistical Computing). http://www.R-project.org/.

Radtke, N.D., Aramant, R.B., Petry, H.M., Green, P.T., Pidwell, D.J., and Seiler, M.J. (2008). Vision improvement in retinal degeneration patients by implantation of retina together with retinal pigment epithelium. Am. J. Ophthalmol. *146*, 172–182.

Redmond, T.M., Yu, S., Lee, E., Bok, D., Hamasaki, D., Chen, N., Goletz, P., Ma, J.X., Crouch, R.K., and Pfeifer, K. (1998). Rpe65 is necessary for production of 11-cis-vitamin A in the retinal visual cycle. Nat. Genet. *20*, 344–351.

Santos-Ferreira, T., Llonch, S., Borsch, O., Postel, K., Haas, J., and Ader, M. (2016). Retinal transplantation of photoreceptors results in donor-host cytoplasmic exchange. Nat. Commun. *7*, 13028.

Shirai, H., Mandai, M., Matsushita, K., Kuwahara, A., Yonemura, S., Nakano, T., Assawachananont, J., Kimura, T., Saito, K., Terasaki, H., et al. (2015). Transplantation of human embryonic stem cell-derived retinal tissue in two primate models of retinal degeneration. Proc. Natl. Acad. Sci. USA *113*, 201512590.

Singh, M.S., Charbel Issa, P., Butler, R., Martin, C., Lipinski, D.M., Sekaran, S., Barnard, A.R., and MacLaren, R.E. (2013). Reversal of end-stage retinal degeneration and restoration of visual function by photoreceptor transplantation. Proc. Natl. Acad. Sci. USA *110*, 1101–1106.

Specht, D., Wu, S.-B., Turner, P., Dearden, P., Koentgen, F., Wolfrum, U., Maw, M., Brandstätter, J.H., and Tom Dieck, S. (2009). Effects of presynaptic mutations on a postsynaptic Cacna1s calcium channel colocalized with mGluR6 at mouse photoreceptor ribbon synapses. Invest. Ophthalmol. Vis. Sci. *50*, 505.

Stan Development Team. (2016a). Stan: A C++ Library for Probability and Sampling, Version 2.10.0. http://mc-stan.org/.

Stan Development Team. (2016b). RStan: the R interface to Stan. http://mc-stan.org/.

Travis, G.H., Ruiz, A., Radu, R.A., Jin, M.–H., and Mata, N.L. (2005). Chicken retinas contain a retinoid isomerase activity that catalyzes the direct conversion of all-trans-retinol to 11-cis-retinol. Invest. Ophthalmol. Vis. Sci. *46*, 1062.

Tummala, S.R., Neinstein, A., Fina, M.E., Dhingra, A., and Vardi, N. (2014). Localization of Cacna1s to ON bipolar dendritic tips requires mGluR6-related cascade elements. Invest. Ophthalmol. Vis. Sci. *55*, 1483–1492.

West, E.L., Pearson, R.A., Barker, S.E., Luhmann, U.F.O., Maclaren, R.E., Barber, A.C., Duran, Y., Smith, A.J., Sowden, J.C., and Ali, R.R. (2010). Long-term survival of photoreceptors transplanted into the adult murine neural retina requires immune modulation. Stem Cells *28*, 1997–2007.